ELSEVIER

Contents lists available at ScienceDirect

International Journal of Fatigue

journal homepage: www.elsevier.com/locate/ijfatigue





Experimental characterization of fatigue life of ZrB₂-SiC based ultra high-temperature ceramic matrix composites

T. Reimer^{a,*}, G.D. Di Martino^a, D. Sciti^b, L. Zoli^b, P. Galizia^b, A. Vinci^b, M.A. Lagos^c, N. Azurmendi^c

- ^a DLR Institute of Structures and Design, Pfaffenwaldring 38-40, 70569 Stuttgart, Germany
- ^b National Research Council, Institute of Science and Technology for Ceramics, Via Granarolo 64, 48018 Faenza, Italy
- c TECNALIA, Basque Research and Technology Alliance (BRTA), Mikeletegi Pasealekua 2, 20009 Donostia-San Sebastián, Spain

ARTICLE INFO

Keywords: Vibration test Experimental methodology Ultra High-Temperature Ceramic Matrix Composites

ABSTRACT

The development process of new Ultra High-Temperature Ceramic Matrix Composites (UHTCMC) for use in severe environments typical of space applications, such as thermal protection or rocket components, still lacks useful data for what concerns the properties influencing the structural behavior under the different load conditions. In particular, the fatigue life of the material plays a fundamental role in the design of full systems determining their resistance to typical vibrational loads. However, this property has been rarely investigated for UHTCMCs and its experimental characterization presents uncertainties related to the materials specific behavior, which does not allow the application of traditional methodology employed for isotropic materials. In the present work, two different methodologies are proposed and applied to new ZrB2-SiC-based UHTCMCs, with either short or long continuous fibers, yielding in combination with numerical analyses to the determination of the σ/N curve for the two classes of materials.

1. Introduction

There are certain applications in spacecraft that require special materials due to the extreme environments. As an example, vehicles returning to earth from space pass through the atmosphere at high velocity, thus generating an environment of super-heated plasma in front which creates the need for a thermal protection system (TPS). Another example is the engine of a chemical rocket burning fuel with an oxidizer and thus creating an extremely hot exhaust gas exiting the thrust chamber at high speed via the nozzle throat [1–3]. These two potential applications were chosen as the target of the development of new materials during the C³HARME project. In the C³HARME project, funded by the European Union, new Ultra-high Temperature Ceramic Matrix Composite (UHTCMC) materials were to be developed to TRL of 6. The materials under development were UHTCMCs based on carbon fibers embedded in a matrix consisting predominantly of zirconium diboride and silicon carbide [4,5] but also containing small amounts of other

additions (self-healing phases [6] and/or sintering aids [7]).

The two target applications have in common the environment of extreme high temperature. In the case of the TPS of a re-entry capsule, the temperatures can vary over a wide range, depending on the capsule size, shape and mass, as well as on the trajectory profile. Temperatures in the range of 2000° C are not uncommon in the case of a low-earth orbit return, when returning from the Moon or even beyond, temperatures can reach even higher numbers [8].

The environmental conditions in the nozzle throat of a rocket engine are also very harsh. In this case the conditions are characterized by very high temperature, high pressure and a high flow velocity of a chemically aggressive combustion gas [9,10].

In addition to the challenging thermal environment, the envisaged structures of TPS panels or nozzle throat components are also subjected to a severe dynamic mechanical load environment [11]. It is the result of a combination of fluctuating mechanical loads coming from the rocket engine itself but also from turbulent aerodynamic pressure loads and

Abbreviations: ASD, Acceleration spectral density; C3HARME, Next Generation Ceramic Composites for Combustion Harsh Environments and Space; CMC, Ceramic Matrix Composite; CNR, Consiglio Nazionale delle Ricerche; DLR, Deutsches Zentrum fuer Luft- und Raumfahrt; PSD, Power spectral density; SiC, Silicon carbide; SPS, Spark plasma sintering; SRTD, Sine resonance track and dwell; TPS, Thermal Protection System; TRL, Technology Readiness Level; UHTCMC, Ultra High Temperature Ceramic Matrix Composite; ZrB2, Zirconium diboride.

E-mail address: thomas.reimer@dlr.de (T. Reimer).

^{*} Corresponding author.

inertia loads [12]. Thus, the lifetime of such materials depends greatly on the magnitude of these loads and on the capability of the materials to withstand them. The issue of the component lifetime is even more important when thinking about a possible re-usability of components on re-usable launch vehicles, foreseen to do 10, 50 or even 100 flights without exchanging the components.

While the fatigue behavior of classical isotropic materials has been widely studied over a long period of time [13], only more recently researchers focused on the characterization of the response of ceramics and Ceramic Matrix Composites (CMC) under mechanical cyclic loads, which, although they are often designated as fatigue insensitive, suffer from fatigue loads as well [14,15]. Moreover, traditional methods used for isotropic materials cannot be directly applied for CMC structures, both because of the unique behavior of ceramics, which do not yield plastically under high loads and are usually high susceptible to flaws, and for the lack of experimental standard procedures and reliable failure criteria [16,17]. The uncertainties are even more significant for the fatigue behavior of UHTCMC materials, on which only few works can be found in the competent literature [18,19].

This work focuses on the UHTCMCs, consisting in a ZrB2-SiC-based matrix reinforced with short or continuous carbon fibers, developed in the framework of the Horizon 2020 European project C³HARME. While a number of studies have been published on the new UHTCMCs developed in the framework of the C³HARME project focusing on the manufacturing process [4,20], on different static mechanical testing [21,22] and on the high-temperature response in representative flows [10,23], the present paper describes the activities aimed at the characterization of the UHTCMC materials under vibrational loads. For this purpose, bending vibration tests at relatively high frequencies have been carried out with a shaker system in two different suitable operating modes and at different load levels in order to determine the fatigue life of the material. An adapted sample shape was chosen for the tests based on the fixed cantilever beam type with increasing cross section towards the clamping to make sure the peak stress is always far from the clamp. In order to define the material degradation and failure, the profile of the resonance frequency has been monitored during the time, similarly to what was done in a previous work [17], while dedicated finite element analyses have been performed to fully characterize the stress field acting in the body for each operating condition.

2. Materials and methods

2.1. Materials

UHTCMCs arise from the combination of ultra-high temperature ceramics (e.g. borides and carbides of early transition metals) and carbon fibers [20]. In the bulk, fibers provide the structural stability and damage tolerance to the components [21,22,24], whilst on the surface the matrix provides protection for the fibers, forming a protective layer upon exposure to aggressive environments [25].

UHTCMCs can be produced with both short and continuous fibers, resulting in products with remarkably different mechanical performance [21,26].

Two large discs with a diameter of 400 mm consisting in a ZrB₂-SiC ceramic matrix with either short random or aligned continuous pitch-based carbon fibers were prepared by ISTEC (continuous fibers) and Tecnalia (short fibers) researchers and subsequently sintered by a spark plasma sintering from a Spanish company, NANOKER (SPS furnaces HPD25, FCT System GmbH, Germany). Details are reported below.

Short fiber reinforced composites were obtained by wet milling a $\rm ZrB_2+10$ vol% SiC powder mixture with short carbon fibers (Nippon Graphite Fiber Corporation, HC-600) to obtain a composite with a total fiber content of 40 vol%. The powder mixture was consolidated by spark plasma sintering (SPS) in vacuum (10–2 Pa) at 2173 K, using a pressure of 50 MPa and with a holding time of 5 min.

Continuous fiber UHTCMCs were fabricated infiltrating

unidimensional carbon fabrics with water-based slurries containing a mixture of $\rm ZrB_2/SiC$ powder and subsequently stacking layers in $\rm 0/90^\circ$ configurations. Consolidation was obtained by SPS with the sintering conditions reported in [27].

After sintering, the bulk density was determined by the Archimedes method, whilst the porosity was measured by image analysis on cross section micrographs. The microstructures were analysed by field emission scanning electron microscopy (FE-SEM, Carl Zeiss Sigma NTS GmbH Öberkochen, Germany). The following mechanical properties were measured.

- \bullet Young's modulus (*E*) and shear modulus using the resonance frequency method (ASTM E1875 08) on 60 mm \times 10 mm \times 2,5 mm bars (length, width, and thickness) using an H&P gain-phase analyzer at RT. 6 bars were tested.
- Flexural strength (σ_f) by 3-point bending at room temperature and 1800 °C on 60 mm \times 10 mm \times 2,5 mm (length, width, and thickness) according to EN 658–3:2002 norm.
- Room temperature tensile tests were carried out at DLR in the Zwick-Roell 1475, a standard mechanical test machine on dog bone shaped bars, following the EN 658–1:1999 norm.

Microstructure of the composites with short and long fibers are illustrated in Fig. 1 and Fig. 2, respectively, and their baseline properties are reported in Table 1.

Short fiber UHTCMCs presented a bulk density of 4,1 g/cm3 and the residual porosity estimated by image analysis was around 1 %. Fig. 1a shows the microstructure characterized by randomly distributed fibers within the matrix, while Fig. 1 shows the strong matrix fiber interface obtained. This material presents a bending strength around 135 MPa and a tensile strength around 80 MPa.

Regarding the continuous fiber composites, the material bulk density (Fig. 2a) was 3,5 g/cm3 and the residual porosity estimated by image analysis was as low as 6 %. The $0/90^{\circ}$ texture is shown in Fig. 2b, the cross section of a 90° layer displays a regular distribution of fibers in the matrix, with a strong matrix fiber interface (see Fig. 2c,d,e). Bending and tensile strength gave a value of 185 and 120 MPa, respectively, the measures of the Young's and shear modulus were 135 and 25 GPa, respectively.

2.2. Vibration test experimental setup

Specimens of the above described material have been tested under vibrational load in a shaker facility. The shaker is a TIRA TV 57315/LS-340 system with the main specifications as given in Table 2.

The test setup was chosen to be a beam bending configuration with the beam deflection to be the result of inertial loads introduced by the shaker movement. Relatively large deflection of the sample occurs when the frequency of the shaker movement is near one of the normal mode frequencies of the sample. In the present case the test was designed in order to trigger the frequency of the first normal mode of the sample, which is a deflection of the tip in the case of a simple beam clamped at one end and inducing movement in transverse direction of the beam. There are other options of operating, as e.g. in the second normal mode, as reported in [28], however, for size and simplicity reasons, the first normal mode was selected in this case.

Fig. 3 shows the sketch design and a picture of the sample. The specific size of the sample with the consequential effect on the resonance frequency was the result of the C³HARME project constraints because the available raw material pieces were limited in size. In addition, reaching a resonance frequency between 500 and 1000 Hz was desired in order to achieve acceptable test times when applying low load levels and thus high cycle numbers before failure occurs. Finally, to avoid a stress concentration at the clamped end of the sample, thus possibly triggering failure there at some unclear stress condition, the sample was shaped with a tapered, wider end at the clamping side. In principle, the

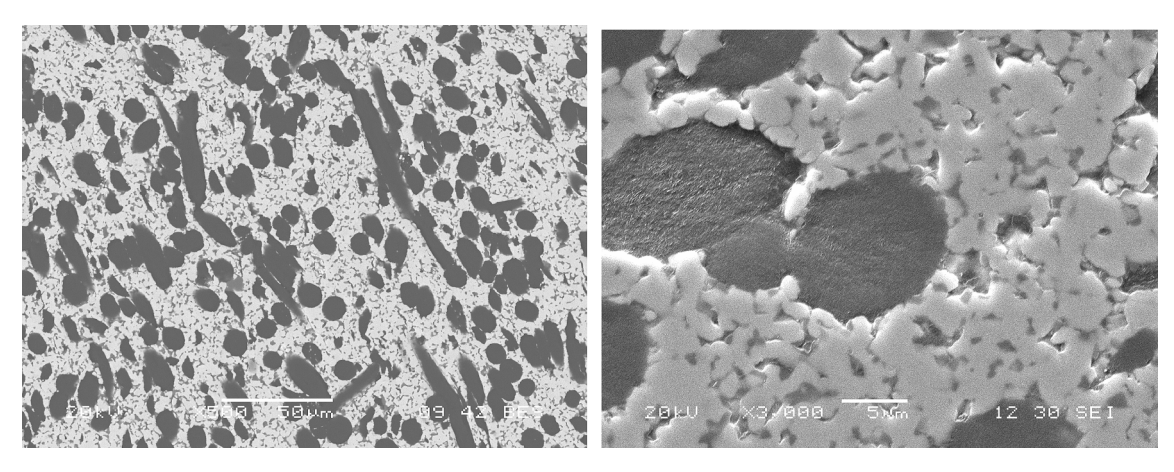


Fig. 1. Microstructure of the short fiber reinforced UHTCs, A) Distribution of fibers, scale bar 50 µm, B) Detail of the interface between matrix and fibers.

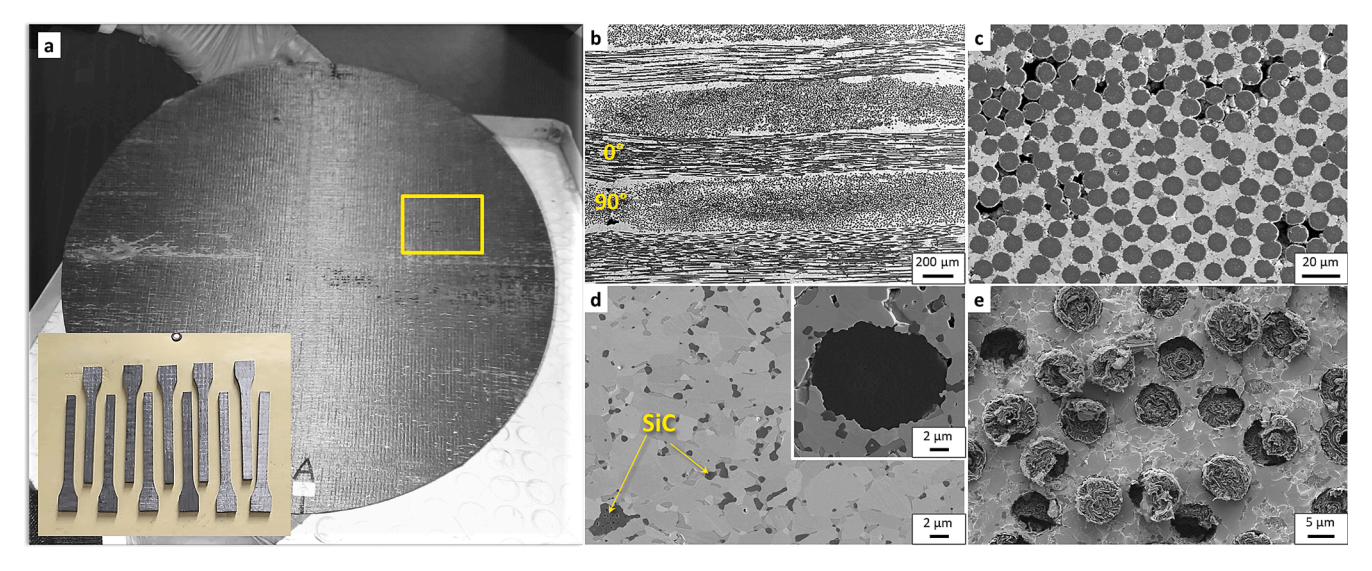


Fig. 2. A UHTCMC disc manufactured by spark plasma sintering, Inset: a) group of vibration tests samples machined from the disc, b) Texture showing the $0/90^{\circ}$ configuration, c) detail of the microstructure showing the homogeneous distribution of fibers, d) polished portion of the matrix material, e) surface section with the fiber pullout.

Table 1
UHTCMCs baseline material properties.

	-	
	Short fibers	Continuous fibers
Architecture	Fibers randomly distributed	0/90°
Density, g/cm ³	$4,1 \pm 0,1$	$3,5\pm0,1$
Porosity, %	1 ± 1	6 ± 3
Fiber amount, %vol.	40 ± 4	54 ± 4
Young's modulus E, GPa	$181\pm2^{\parallel}$	$137\pm6^{\parallel}$
	$81\pm4^{\perp}$	$25\pm3^{\perp*}$
Shear modulus G, GPa	17 ± 1	25 ± 1
RT Flexural strength σ _f , MPa	$135\pm5^{\parallel}$	$185\pm20^{\parallel}$
RT Tensile strength σ_t , MPa	$80\pm18^{\parallel}$	$120\pm7^{\parallel}$

Properties obtained for the direction parallel to the fibers.

taper can be done in two ways, either in the plane of the sample, transverse to the sample deflection, so that the sample becomes wider or by having the sample thicker at the clamping end and keeping the same width all over the length. In the present case, the first option was selected in order to avoid cutting through the top and bottom outer layers of carbon fibers in the sample to achieve the thickness taper.

Table 2 Shaker TIRA TV 57315/LS-340 main specifications.

Rated peak force, N	Sine/Random/Shock	15000/15000/30000
Frequency range, Hz Max. rated travel, mm Max. velocity, m/s Max. acceleration, g Armature diameter, mm	Pk-Pk Sine/Random/Shock Sine/Random/Shock	3000 50,8 1,8/1,8/2,5 100/100/200 340

With the available material data (see Table 1), finite element analysis (FEA) was carried out to determine the resonance frequency and the stress field in the sample. Regarding the shape of the sample the goal was to achieve a stress field where the highest stress is in the region of the tapering, preferably at the onset where the straight section starts to increase in width. In addition, the goal was to achieve a homogeneous stress distribution over the width of the sample. Fig. 4 shows the stress distribution on the sample as a result of the bending. The maximum stress is near the start of the tapering of the sample width as intended.

The clamp design was given close attention since it can have a large influence on the test quality. Two main goals were to be achieved via an appropriate clamp design. First, equal distribution of forces on the sample in the clamping section and avoiding of overstressing the sample

 $[\]square$ Properties measured on bars vertically machined (pile-up direction in case of continuous fibers).

^{*} Value obtained from a similar material [27].

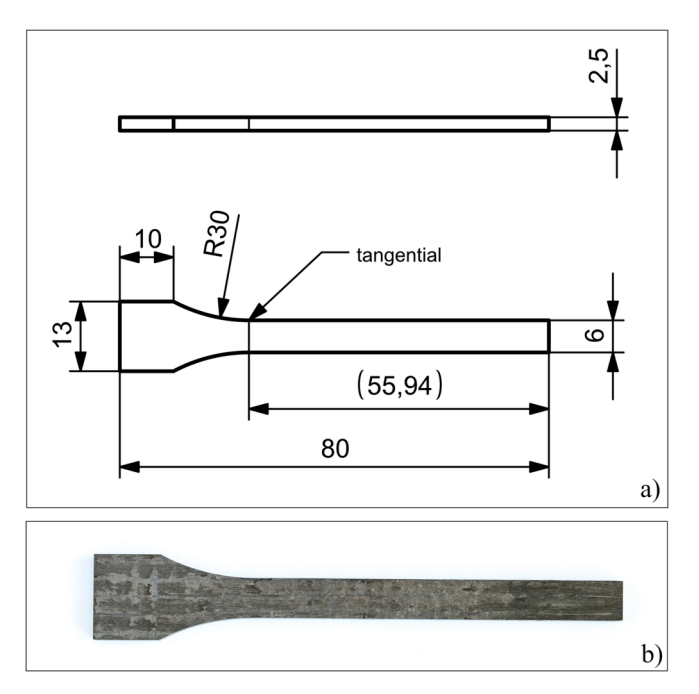


Fig. 3. Vibration test sample: a) nominal dimensions, b) picture of actual long fiber UHTCMC sample.

edges. Second, a reproducible, proper alignment on the shaker. Both goals were achieved via the introduction of a dedicated spacer plate in combination with a suitable tolerancing of both metallic clamping components and the sample itself. On one side of the spacer plate, a rectangular cut-out was present in which the sample was placed as shown in Fig. 5a, so that the position of the sample is always the same with respect to the clamping block and shaker (see Fig. 5a and b). In addition, due to the tight tolerancing of sample and spacer plate with the sample always being a well defined small amount thicker than the spacer, damage to the sample edges and the use of additional tabbing material could be avoided.

The control of the tests was done via an accelerometer (Brüel & Kjaer Charge Accelerometer Type 4382), installed via a stud bolt on the shaker mounting plate. The measurement of the sample tip deflection was done via a laser triangulation sensor ($\mu\epsilon$ LD1625-20) above the sample tip, focused on the sample close to the tip edge as shown in Fig. 5c. In order to achieve good deflection measurements with the laser sensor, the tip of the sample was sprayed with a matte white paint for optimum reflectance.

Two different operating modes were adopted for the vibration tests, which will be referred to as random vibration test and sine resonance

track and dwell (SRTD) test. In particular, the SRTD mode foresees a sinusoidal acceleration input at a fixed frequency, which after a first search phase is locked to the sample resonance frequency. At first it was actually planned to do only SRTD tests with all samples. However, with the short fiber UHTCMC samples the material was already affected during the search phase, with a consequent drop of the resonance frequency, which in turn made impossible to lock on to the resonance frequency. For this reason, the random vibration approach, usually employed for testing complex components, was considered, in which a prefixed range of frequency is excited with random vibration according to the set acceleration spectrum density (ASD) input. This technique is more representative of real load conditions, but suffers of two main drawbacks. First it is more energy expensive, limiting the achievable load levels, which in the present case was not enough to get significant results for the CNR materials. Moreover, for the random nature of the input, it is not possible to get deterministic results, but the characterization can be performed only in statistical terms.

A detailed description of the abovementioned test procedures is given in the following sections.

2.3. Test procedures and matrix

2.3.1. Random vibration test

In the present work, the random vibration tests were carried out setting for each sample a uniform ASD over the frequency range of interest. The baseline frequency range was set from 100 Hz to 1000 Hz, while only in the test cases at the highest acceleration loads it was narrowed to comply with the shaker power capability limits.

During each test the corresponding signal measured by the laser is monitored during the time and processed by the system in order to get the spectrum of the displacement at the tip of the beam specimen. Typically, such a spectrum presented a peak corresponding to the first-mode resonance frequency of the sample: the characteristic of the spectrum profile around the resonance frequency gave a qualitative indication of the state of the material, whose degradation is associated to a broadening of the resonance peak and a reduction of the maximum displacement amplitude [17].

Each random vibration test was divided into several substeps of a prescribed duration, in order to monitor the sample status and the eventual formation and following propagation of a surface crack. The total number of load cycles was determined as the cumulative sum of the number of cycles at the end of each substep.

Failure in the random vibration tests was defined as the moment when no significant peak could be detected in the PSD response of the sample, or, in the cases in which this did not happen before the sample failure, as the moment when the sample actually broke in two pieces thus triggering system abort limits.

Table 3 and Table 4 list respectively the short fiber and long fiber

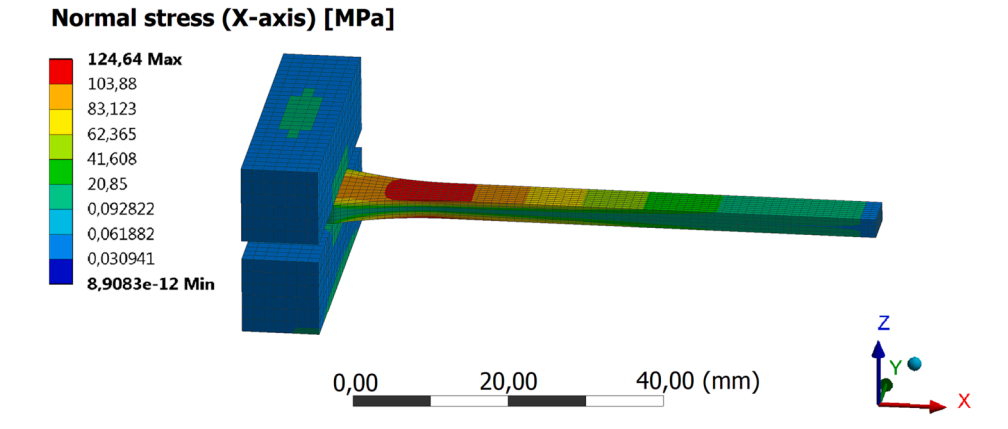


Fig. 4. FEA result of harmonic analysis, giving the stress field due to bending vibration at first resonance frequency.

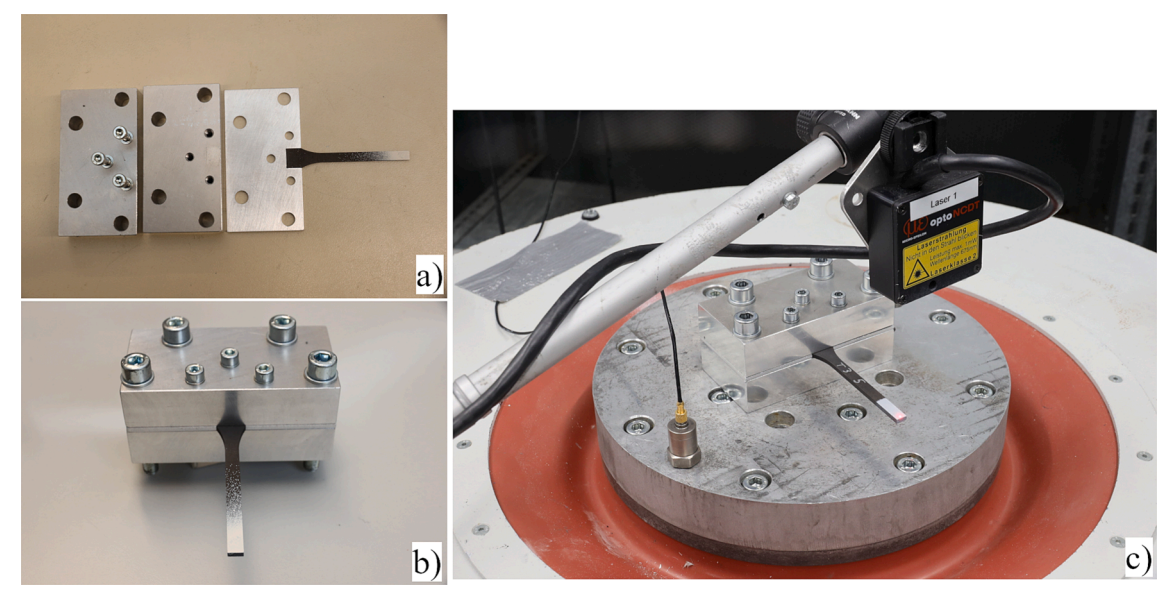


Fig. 5. Vibration test clamping and setup: a) clamping block parts, b) assembled clamping block with installed sample, c) Test setup with sample installed in clamping blocks, control accelerometer and measurement laser.

UHTCMC samples tested in the random vibration mode and the corresponding nominal loads at which they have been tested, in terms of the level of the uniform ASD and the frequency range. It can be noticed that mainly short fiber material samples were tested in the random vibration mode, allowing the full characterization in this operating environment. The reason for this is that, as it will be shown in the following, long fiber material samples showed a more stable response and a corresponding longer fatigue life never reaching failure, not even at the system highest load capability.

2.3.2. Sine resonance track and dwell test

As anticipated before, in order to achieve higher load levels, the SRTD test mode was adopted. In this case the acceleration input signal has a sinusoidal profile at a fixed frequency which is the resonance frequency at the first mode. In practice, although the approximate value of the first-mode resonance is known from the material data and the sample geometry, the exact frequency needs to be determined at the start of each individual test. Thus, in the starting phase of the experiment, the system scans a prescribed frequency range around the expected resonance in order to find the resonance frequency, based on the evaluation of the phase shift between the signal of the control accelerometer and the signal measured at the sample tip by the laser sensor. Once the resonance frequency is found, the system sets the phase shift between the profiles of the acceleration input and the displacement response at the tip of the sample as its control target and tries to

Table 3Short fiber UHTCMC random vibration test matrix.

UHTCMC sample ID	Frequency range, Hz	ASD level, g ² /Hz	UHTCMC sample ID	Frequency range, Hz	ASD level, g ² /Hz
SF-R-1	100-1000	0,2	SF-R-12	100-1000	0,5
SF-R-2	100-1000	0,25	SF-R-13	100-1000	0,5
SF-R-3	100-1000	0,25	SF-R-14	100-1000	0,5
SF-R-4	100-1000	0,3	SF-R-15	100-1000	0,6
SF-R-5	100-1000	0,3	SF-R-16	100-1000	0,6
SF-R-6	100-1000	0,3	SF-R-17	100-1000	0,6
SF-R-7	100-1000	0,4	SF-R-18	100-1000	0,7
SF-R-8	100-1000	0,4	SF-R-19	100-1000	0,7
SF-R-9	100-1000	0,4	SF-R-20	100-1000	0,8
SF-R-10	100-1000	0,4	SF-R-21	100-1000	0,82
SF-R-11	100-1000	0,5	SF-R-22	100-600	1,0

Table 4Long fiber UHTCMC random vibration test matrix.

	UHTCMC sample ID	Frequency range, Hz	ASD level, g ² /Hz	UHTCMC sample ID	Frequency range, Hz	ASD level, g ² /Hz
_	LF-R-1	150-700	1,0	LF-R-2	325-625	2,0

maintain this value. In this way, the sinusoidal input adapts in order to follow an eventual change of the resonance frequency, depending on the material mechanical characteristics and its structural integrity.

In the present case, in order to avoid significant change in the resonance frequency during the search phase at the beginning of each run, the resonance search is performed at a low load level of typically $10 \, \text{m/s}^2$. Once the resonance frequency is identified, there is a stepwise increase of the load level up to the target value in terms of increasing acceleration input up the next-to-last load level. In particular, in this case the target load level is defined by notching the maximum displacement at the tip to a set value, which is controlled by the system, eventually adjusting the amplitude of the acceleration input, in order to get a constant maximum deflection, and thus, stress in the body which is then kept for a prescribed number of cycles.

In the case of the SRTD tests, the procedure itself allows to constantly monitor the resonance frequency, the tip displacement and the acceleration input of the sample during the run. The failure criterion is then defined as the moment in which the first abrupt change in the resonance frequency is detected.

Table 5 reports the plan for the SRTD tests. On the contrary to the random tests, in this case only few short-fiber UHTCMC samples were tested in the SRTD mode, while a full characterization was possible in the case of the long-fiber material. Moreover, a second batch of CNR samples are included in the matrix, which, differently to the other ones that all had the nominal dimensions showed in Fig. 3, were obtained by thinner leftover material plates and consequently presented a different thickness, as also reported in Table 5.

2.4. Numerical models

In order to support the experimental characterization, numerical analyses have been carried out with the commercial tool ANSYS Mechanical with the main purpose of estimating the stress distribution in

Table 5Long fiber UHTCMC SRTD test matrix.

UHTCMC sample ID	Thickness, mm	Nominal displacement, mm	UHTCMC sample ID	Thickness, mm	Nominal displacement, mm
LF-SD-1	2,5	0,2	LF-SD-9	2,5	1,7
LF-SD-2	2,5	0,6	LF-SD-10	2,1	1,9
LF-SD-3	2,5	0,9	LF-SD-11	2,05	2,1
LF-SD-4	2,5	1	LF-SD-12	2,15	2,2
LF-SD-5	2,5	1,2	LF-SD-13	2,0	2,4
LF-SD-6	2,5	1,5	LF-SD-14	2,0	2,5
LF-SD-7	2,5	1,6	LF-SD-15	2,05	2,5
LF-SD-8	2,5	1,7	LF-SD-16	2,1	2,6

the sample for each test.

Fig. 6 shows the meshed sample geometry considered for the numerical simulations. The modelling of the complete experimental apparatus, including the interface plate to the shaker, the clamping block and the bolted connection with the consequent pretensional status, has been preliminary assessed to have a negligible effect on the simulation results and therefore has not been considered.

For all the simulations, a fixed boundary condition is set on the sample bottom and up surfaces in the clamping zone (highlighted in Fig. 6).

A specific discussion is needed for the mechanical properties of the new UHTCMC materials set for the numerical calculations. In fact, as it will be discussed in detail in the following sections, because of the composite nature of the material and the fact that the production processes are still under development which still leave the possibility of local dishomogeneity, the samples presented an uneven behavior in terms of the initial resonance frequency, for fixed load and geometry, which can be attributed to differences in the local value of the Young's modulus. Moreover, the differences in the initial resonance frequency occur also changing the load level, because of the nonlinear behavior of the materials (see for example [27], in the case of the long fibers material) in the range of considered stresses and of eventual damping effects (not explicitly taken into account in the simulations).

In order to reduce the scattering due to the abovementioned factors, a preliminary parametric modal analysis has been carried out to get a correlation between the material Young's modulus and the resonance frequency of the sample first vibrational mode. The results of these analyses for the 2,5-mm thickness samples are shown in Fig. 7. Similar results were obtained also for the CNR sample of different thickness, considering also their slight differences in terms of density (which were anyway in the order of \pm 3 %). Thus, for each test the initial resonance frequency at the prescribed load was detected and the corresponding elastic modulus was set for the carrying out the numerical simulation.

For what concerns the random vibration tests, the numerical study is performed in two steps. First a modal analysis is carried out for natural frequency and mode shape determination, under the simplifying assumptions that the structure has constant stiffness and mass effects, while there is no damping. The characterization of the natural vibration modes is needed for the definition and solution of the random vibration simulation with the Power Spectral Density (PSD) approach, combined with mode-superposition techniques [29]. For the PSD analyses the load in terms of the ASD considered in each test is applied.

On the other side, since the SRTD tests do not have a random nature,

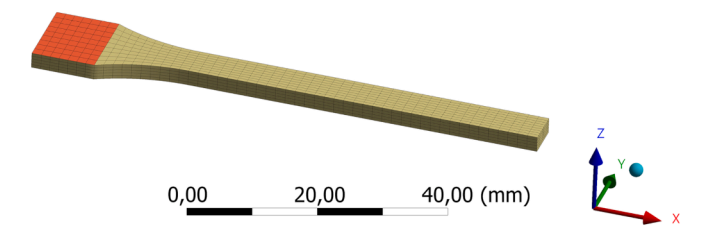


Fig. 6. Geometry and mesh for vibration test numerical simulations.

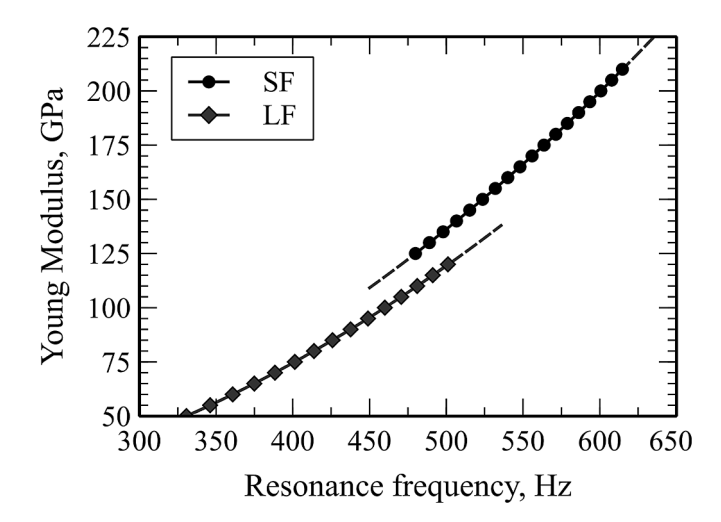


Fig. 7. Correlation between material elastic modulus and resonance frequency of the sample first vibrational mode.

being characterized by a well-defined sinusoidal input, whose settings were defined in order to have a practically constant maximum displacement amplitude, a simplified approach could be used in this case, considering simple static mechanical simulations. Thus, in order to recreate the same stress distribution acting in the sample in the moment of maximum oscillation amplitude, an acceleration load was prescribed setting for it a value that allows to obtain the maximum displacement at the tip considered for each test.

3. Fatigue behavior of short-fiber UHTCMCs

As anticipated in $Sec.\ 2.3.1$, a total of 22 samples of UHTCMC reinforced with short fibers have been tested in random vibration mode.

The test procedure allowed for each test to get the displacement spectral response, measured at the tip of the sample, at different times during the test. Fig. 8 shows the evolution of the spectral response during the time for two example tests, SF-R-4 and SF-R-11, carried out at $0.3 \text{ g}^2/\text{Hz}$ and $0.5 \text{ g}^2/\text{Hz}$ respectively. As anticipated before, it can be clearly noticed that the displacement peak due to the resonance phenomena at the frequency of the sample first vibrational mode changes in time with a reduction of the maximum value and a broadening of the frequency range of interest. This can be associated to a loss of stiffness of the sample due to the progressive material degradation. Moreover, as it can be expected, the rate of the abovementioned behavior is faster for a higher load level. At some point no significant resonance peak is detectable anymore; although, in both cases the test went on for some minutes more before the sample completely broke into two pieces, the first time instant in which the displacement spectral density showed no resonance peak was considered to be the time of material failure.

This can be supported looking at the pictures of the samples around the critical zone taken after different test substeps, shown for the example test SF-R-4 and SF-R-11 in Fig. 9 and Fig. 10, respectively. In

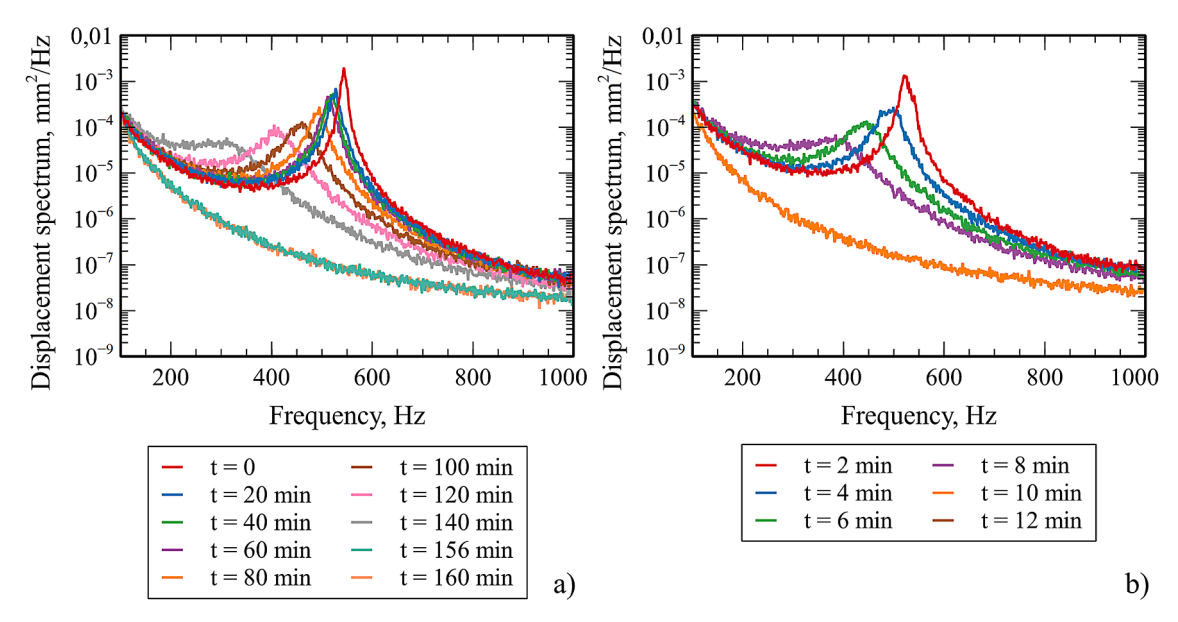


Fig. 8. Displacement spectral density during random vibration test: a) SF-R-4, b) SF-R-11.

the test SF-R-4 no signs of material damage could be observed until roughly 145 min, when the first hint of a crack was slightly visible, starting from the lower side of the sample, in particular on a spot where the sample presented already a geometrical flaw. The crack became evident at 156 min from the test start, corresponding to the instant at which the displacement spectral density showed no peak anymore (Fig. 8a) and the failure criteria was met. The test went on for some minutes before the sample broke in two pieces. Similarly, in the test SF-R-11, the crack became evident after 10 min from the test start corresponding also in this case to the instant in which the displacement spectrum showed no peak (Fig. 8b). In this case it was possible to continue the test for a while until the sample broke.

An overview of the test results in terms of the ASD level and the time before failure is graphically shown in Fig. 11. As expected, although the scattering of the data, it is already clear the decreasing power correlation between the load level and the material fatigue life.

As described in *Sec.* 2.4, each test condition was numerically simulated with the main aim of estimating the statistical stress distribution in the sample. Fig. 12 shows for the test case SF-R-11 the contour plot of the 3- σ local normal stress in the direction of the sample length, i.e. at each point the actual instantaneous normal stress in the length direction in modulus will lie below the displayed value with a probability of 99,7%. It can be noticed that, as desired, the maximum stress is reached in the region at the end of the tapering and in particular on the up and bottom

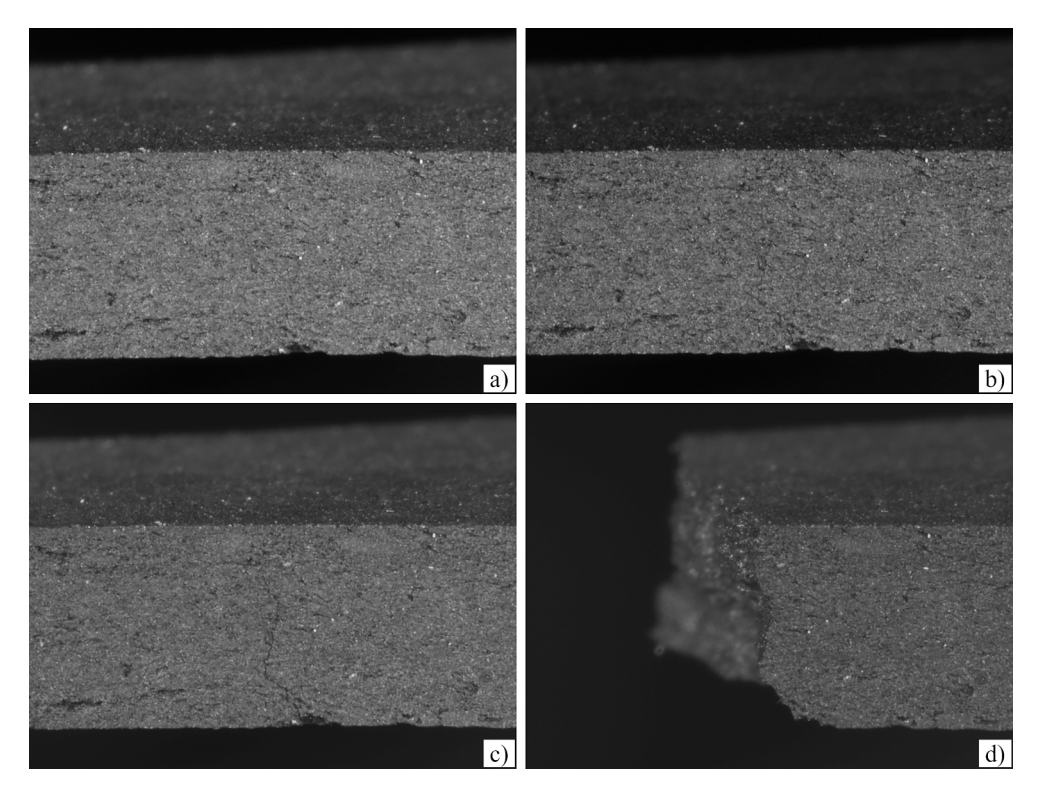


Fig. 9. Crack propagation during test SF-R-4: a) t = 0, b) t = 145 min, c) t = 156 min, d) t = 160 min.

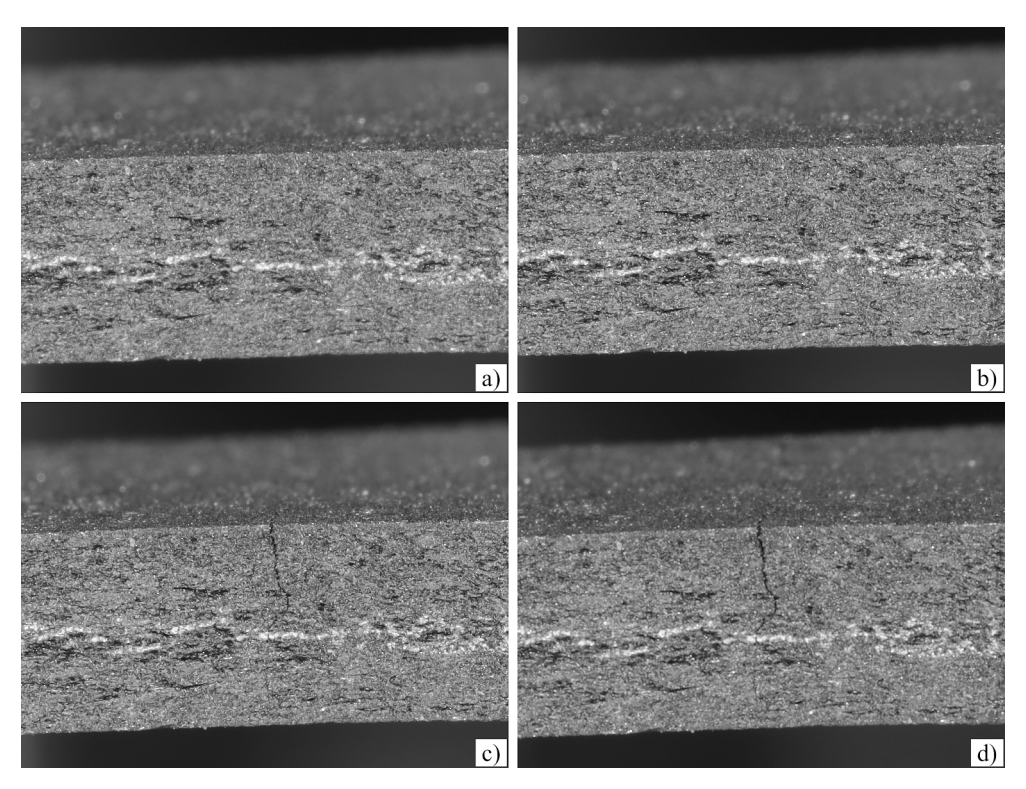
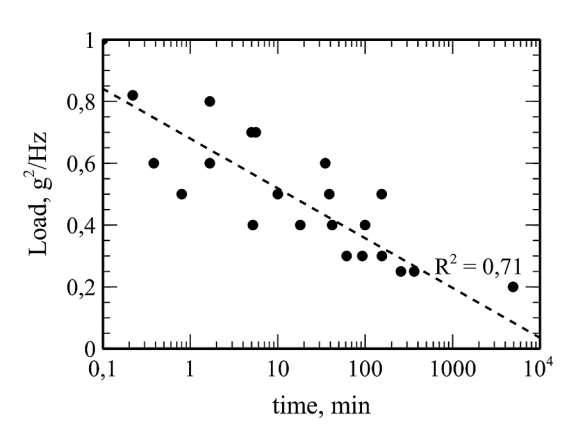


Fig. 10. Crack propagation during test SF-R-11: a) t = 0, b) t = 6 min, c) t = 10 min, d) t = 25 min.



surfaces. In fact, since the displayed values are in absolute value, these are the regions where the maximum tension and the maximum compression alternate during the vibration, according to the typical transversal stress distribution for a cantilever beam subject to flexure.

For each test, then, the maximum 3- σ normal stress in the length direction was calculated and considered to be representative of the stress level condition in the sample. The results are summarized in Table 6 and graphically displayed in Fig. 13. It is worth noticing that the values of the Young's modulus obtained as described in *Sec.* 2.4 are in line with the reference data in Table 1. From Fig. 13 it is also possible to notice that the numerical modelling allowed to partly reduce the scattering of the data.

4. Fatigue behavior of long-fiber UHTCMCs

4.1. Random vibration tests

As anticipated in *Sec.* 2.3.1, only two samples of continuous-fiber UHTCMC samples were preliminary tested in random vibration mode. It was found that, although the acceleration spectrum density was

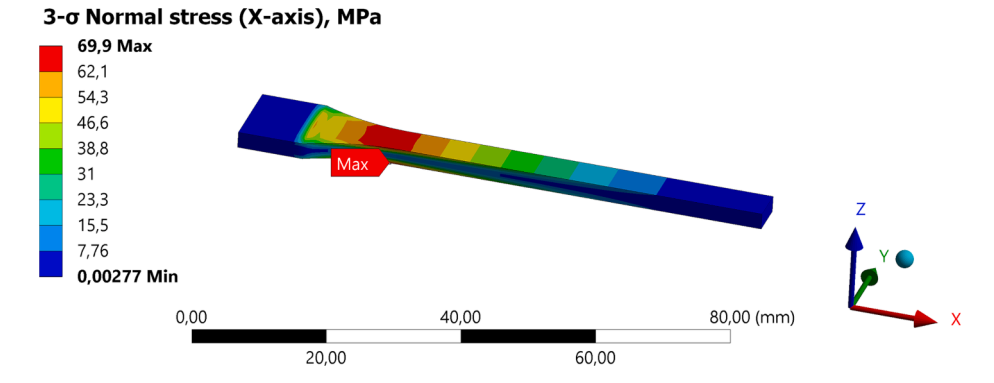


Fig. 12. Numerically calculated 3- σ normal stress distribution in the sample during test SF-R-11.

Table 6Short fiber UHTCMC random vibration tests main results.

UHTCMC sample ID	Frequency range, Hz	ASD level, g ² / Hz	Initial resonance frequency, Hz	Young's modulus, GPa	$3\text{-}\sigma$ maximum normal stress, MPa	Time before failure, min
SF-R-1	100-1000	0,2	550	166,2	46,1	4920
SF-R-2	100-1000	0,25	562	173,9	52,3	362
SF-R-3	100-1000	0,25	550	166,2	51,6	255
SF-R-4	100-1000	0,3	544	162,4	56,1	156
SF-R-5	100-1000	0,3	550	166,2	56,5	93
SF-R-6	100-1000	0,3	553	168,1	56,7	61,5
SF-R-7	100-1000	0,4	565	175,8	66,3	18,1
SF-R-8	100-1000	0,4	563	174,5	66,2	5,18
SF-R-9	100-1000	0,4	513	143,6	62,6	100
SF-R-10	100-1000	0,4	537	158,1	63,3	42
SF-R-11	100-1000	0,5	520	147,8	69,9	10
SF-R-12	100-1000	0,5	560	172,6	73,8	155
SF-R-13	100-1000	0,5	490	130,5	68,1	38,9
SF-R-14	100-1000	0,5	559	171,9	71,4	0,8
SF-R-15	100-1000	0,6	585	189,1	82,9	0,383
SF-R-16	100-1000	0,6	570	179,1	81,6	1,68
SF-R-17	100-1000	0,6	504	138,4	75,9	35
SF-R-18	100-1000	0,7	522	149,0	83,0	5,6
SF-R-19	100-1000	0,7	545	163,1	85,2	5
SF-R-20	100-1000	0,8	527	152,0	88,8	1,68
SF-R-21	100-1000	0,82	559	171,9	94,3	0,22
SF-R-22	100-600	1,0	560	172,6	104,3	0,1

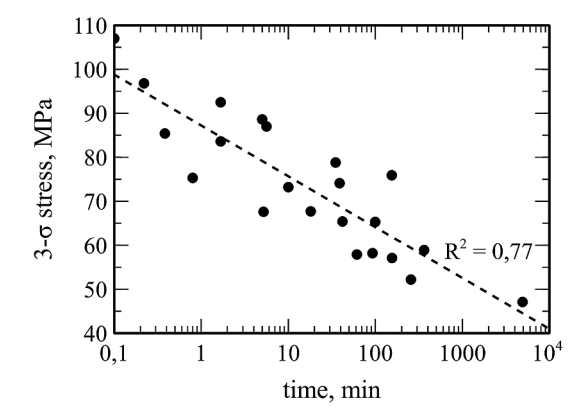


Fig. 13. Short fiber UHTCMC random vibration: 3- σ normal stress vs time before failure.

increased, decreasing the frequency range, in order to comply with the power limit of the shaker system for this kind of test, it was not possible to get a failure for these composites.

Table 7 reports the main results of the tests and the relative simulations, while Fig. 14 shows the displacement spectral response at the tip of the two samples at the beginning and at the end of the tests, which did not significantly change in both cases, demonstrating that after the 24 h of test the material was practically unaffected.

The above-described results already prove that long-fiber UHTCMC are characterized by a more performant fatigue life with respect to the short-fiber material.

4.2. Sine dwell tests

In order to get more information about the fatigue life also for the

long-fiber material, another experimental campaign with the SRTD mode was carried out, which is described in the following section.

Fig. 15 plots the measured data for Test LF-SD-13 as an example of the SRTD test run. In this case the test consisted of two different substeps. In both cases the run started with the search of the resonance frequency followed by stepwise increase of the load that allowed the material to gradually adapt up to the nominal operating conditions (dashed lines in Fig. 15). In particular, in this phase a decrease of the lock frequency was observed due again to the non-linear behavior of the material. Finally, when the nominal value of the maximum displacement was reached, the load input and the frequency stabilized on a constant value and the stationary phase of the test started (solid lines in Fig. 15), which is the only part considered in the computation of the total number of cycles.

For the considered test, the stationary phase in the first substep lasted for around 1 million cycles without significant effects. Nevertheless, during the second substep, a first non-critical effect in the material could be detected after around $5\cdot10^5$ cycles, while after around $6.5\cdot10^5$ cycles an abrupt reduction of the maximum displacement could be observed, followed by a change in the slope of the frequency (simultaneously the input load suddenly increases since it is not limited anymore by the notch of the displacement). From this moment, the system was not able to recover the nominal conditions anymore, meaning that the sample had lost its structural resistance (the sample physically broke after few more thousands of cycles).

As described before, also in this case numerical simulations were carried out to characterize the stress field in the sample, in particular in the moment of maximum deflection. Fig. 16 shows the results for the test LF-SD-13.

Similar results were obtained for the other samples in order to get a correlation between the maximum operating stress and the number of cycles before failure, despite the difference of thickness and the inhomogeneities among the samples. These main results are summarized in Table 8 and shown graphically in Fig. 17. The fitting line in Fig. 17 is

Table 7Long fiber UHTCMC random vibration tests main results.

UHTCMC sample	Frequency range,	ASD level, g ² /	Initial resonance frequency,	Young's modulus,	$3\text{-}\sigma$ maximum normal stress, MPa	Time before failure,
ID	Hz	Hz	Hz	GPa		min
LF-R-1	150–700	1,0	490	114,3	85,8	No failure
LF-R-2	325–625	2,0	464	101,9	116,6	No failure

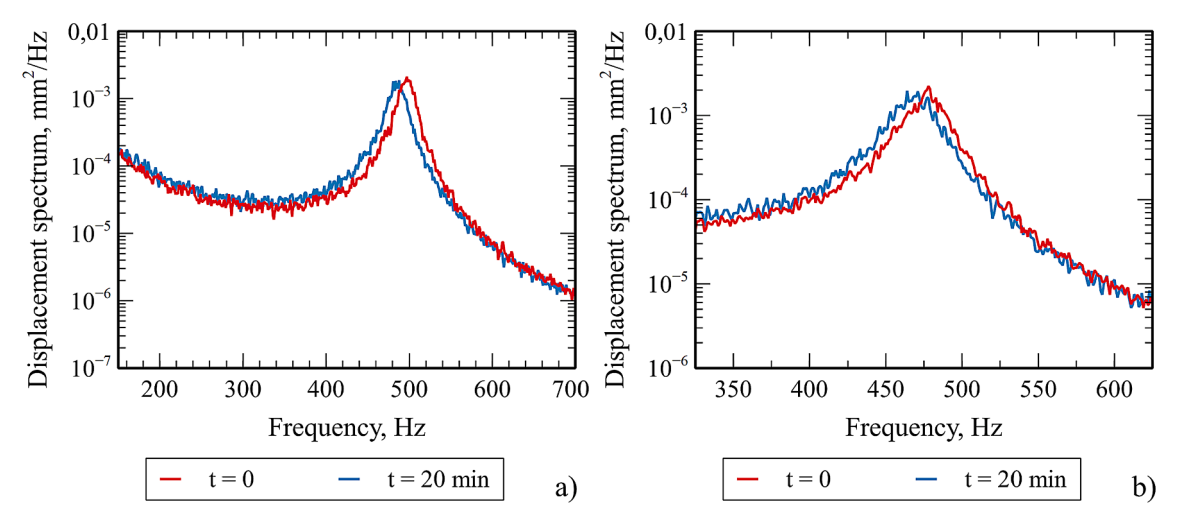


Fig. 14. Displacement spectral density during random vibration test: a) LF-R-1, b) LF-R-2.

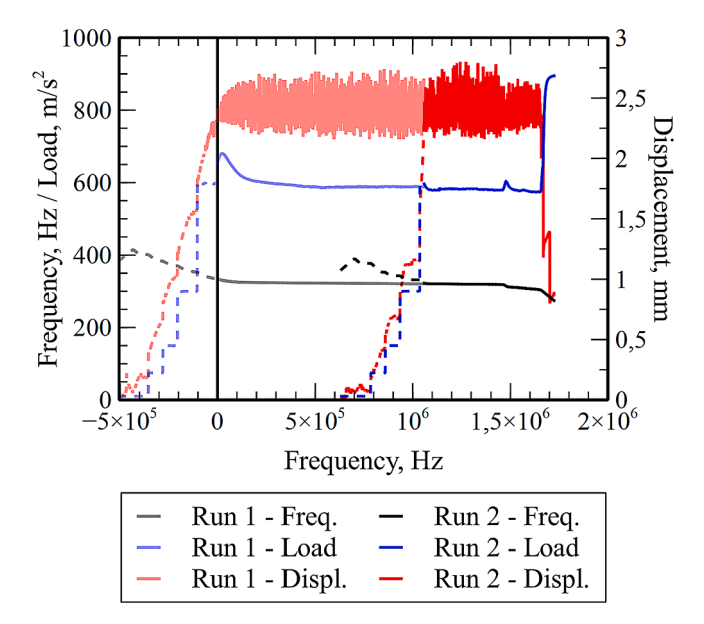


Fig. 15. Test LF-SD-13 run (dashed line: preliminary resonance frequency phase; solid line: test run).

calculated considering only the tests where sample failure was actually reached. Moreover, the test LF-SD-15 was considered to be an outliner, its data point falling far from the correlation of the other tests. In these assumptions, the obtained data show a clear trend.

5. Conclusions

In the framework of the European project ${\rm C}^3$ harme, new UHTCMC materials based on a ${\rm ZrB_2}$ -SiC matrix reinforced with either short or long carbon fibers are developed, characterized and validated for harsh aerospace applications. In this process the full characterization of the material properties is very important, especially in view of application as reusable components, in terms of fatigue life and of resistance to vibrational loads, which could arise due to the rocket engines operation or to the fluid–structure interaction in the reentry phase. However, in the reference literature there is no defined methodology for this purpose. In the present work, two different methods for vibration test of the new UHTCMCs were considered and applied according to the material samples response.

In particular, the random vibration was carried out on short fiber UHTCMC, setting for each sample a uniform ASD over the baseline frequency range of interest between 100 and 1000 Hz. The observation of the resulting displacement spectrum response allowed the evaluation of the material response up to the sample failure, that was defined as the moment in which the peak associated to the sample first mode resonance was not recognizable anymore. On the other side, for the long fiber UHTCMC the SRTD method was applied in which the acceleration input signal has a sinusoidal profile at a fixed frequency which is the first mode resonance frequency of the sample. In this case, the material failure was

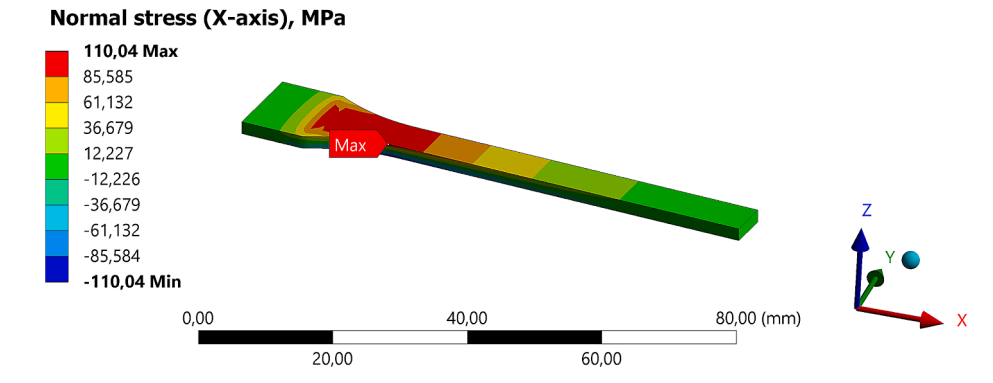


Fig. 16. Numerically calculated normal stress distribution in the sample corresponding to maximum displacement during test LF-SD-13.

Table 8
Long fiber UHTCMC SRTD test main results.

UHTCMC sample ID	Thickness, mm	Maximum displacement, mm	Resonance frequency, Hz	Young's modulus, GPa	Maximum normal stress, MPa	Number of cycles
LF-SD-1	2,5	0,2	522	132,8	20,0	1,00·10 ⁷
LF-SD-2	2,5	0,6	492	117,2	53,3	$1,00\cdot10^{7}$
LF-SD-3	2,5	0,9	461	102,1	70,0	$1,00.10^7$
LF-SD-4	2,5	1	473	107,8	82,0	$1,00.10^7$
LF-SD-5	2,5	1,2	445	94,8	87,0	$1,00\cdot10^{7}$
LF-SD-6	2,5	1,49	432	89,1	102,5	$1,95 \cdot 10^6$
LF-SD-7	2,5	1,6	430	88,0	108,0	$2,75 \cdot 10^6$
LF-SD-8	2,5	1,68	421	84,5	118,0	$2,48 \cdot 10^5$
LF-SD-9	2,5	1,7	428	87,2	114,5	$4,31\cdot10^4$
LF-SD-10	2,1	1,9	351	83,3	101,8	$1,00\cdot10^{7}$
LF-SD-11	2,05	2,1	337	79,4	106,5	$2,30\cdot10^6$
LF-SD-12	2,15	2,2	318	65,3	94,5	$4,28 \cdot 10^6$
LF-SD-13	2,0	2,4	321	74,2	110,0	$1,65 \cdot 10^6$
LF-SD-14	2,0	2,52	333	81,5	128,0	$5,65\cdot10^4$
LF-SD-15	2,05	2,53	291	58,9	96,2	$1,02 \cdot 10^5$
LF-SD-16	2,1	2,58	343	79,5	131,5	$3,44 \cdot 10^4$

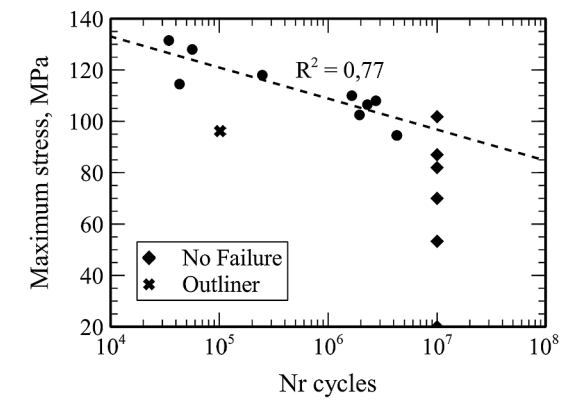


Fig. 17. Long fiber UHTCMC SRTD test: maximum stress vs number of cycles before failure.

associated to an abrupt decrease of the resonance frequency, representing a sudden loss of the material elastic resistance. In both cases, the experiments were supported by numerical simulations, which aimed at calculating from the operating test conditions the corresponding stress distribution in the sample. The numerical analyses allowed to compensate the material inhomogeneities and the non-linear behavior for increasing load conditions. In particular, for the short fibers UHTCMC it was possible to estimate the differences in the elastic properties of the different samples (in average \pm 10 % in terms of the Young's modulus), which improved the quality of the correlation of around 9 % in terms of R^2 . The effect is even more important in the case of the long fibers UHTCMC, where the non-linearity of the material leads for a load case of around 60 % of the flexural maximum strength to a reduction of around 45 % of the Young's modulus.

Finally, for both class of UHTCMCs it was possible to define a clear correlation between the load level to which the sample was subjected and the fatigue life in terms of either the time or the number of cycles before failure. In particular, long fiber UHTCMCs were proven to be more stable and have a better resistance to relatively strong vibrational loads.

It is acknowledged that tests of this kind should be repeated also at high temperature more close to the operating environment. This seems to be feasible by the use of a shaker in combination with a sample heating device. This could be a small furnace chamber where just the sample and the clamping device are placed inside. The clamping device would either need to be produced from CMC material also or it needs to be cooled if it is metallic. DLR can also produce CMC fasteners for use at high temperature to use in the clamping. As an alternative, a laser

heating system seems to be attractive because then the thermal energy could be more efficiently focused on just the sample where the high stress region is located.

Declaration of Competing Interest

The authors declare that they have no known competing financial interests or personal relationships that could have appeared to influence the work reported in this paper.

Data availability

Data will be made available on request.

Acknowledgements

This work has received funding from the European Union's Horizon 2020 "Research and innovation programme" under grant agreement No 685594 (C3HARME).

References

- Weihs H., Longo, J., Gülhan, A.: Sharp Edge Flight Experiment SHEFEX. Fourth European Workshop on Thermal Protection Systems and Hot Structures Conference Proceedings, ESA SP-521 (2002).
- [2] Natali M, Kenny JM, Torre L. Science and technology of polymeric ablative materials for thermal protection systems and propulsion devices: A review. Progress Mater Sci 2016;84:192–275. https://doi.org/10.1016/j. pmatsci 2016.08.003
- [3] Savino R, Criscuolo L, Di Martino GD, Mungiguerra S. Aero-thermo-chemical characterization of ultra-high-temperature ceramics for aerospace applications. J Europ Ceram Soc 2018;38(8):2937–53. https://doi.org/10.1016/j. jeurceramsoc.2017.12.043.
- [4] Zoli L, Sciti D. Efficacy of a ZrB2–SiC matrix in protecting C fibres from oxidation in novel UHTCMC materials. Mater Design 2017;113:207–13. https://doi.org/ 10.1016/j.matdes.2016.09.104.
- [5] Zoli L, Vinci A, Galizia P, Melandri C, Sciti D. On the thermal shock resistance and mechanical properties of novel unidirectional UHTCMCs for extreme environments. Sci Rep 2018;8:9148. https://doi.org/10.1038/s41598-018-27328-
- [6] Silvestroni L, Vinci A, Failla S, Zoli L, Rubio V, Binner J, et al. Ablation behaviour of ultra-high temperature ceramic matrix composites: Role of MeSi2 addition. J Eur Ceram Soc 2019;39(9):2771–81. https://doi.org/10.1016/j. jeurceramsoc.2019.03.031.
- [7] Vinci A, Zoli L, Galizia P, Sciti D. Influence of Y2O3 addition on the mechanical and oxidation behaviour of carbon fibre reinforced ZrB2/SiC composites. J Eur Ceram Soc 2020;40:5067–75. https://doi.org/10.1016/j.jeurceramsoc.2020.06.043.
- [8] Berger KT. Aerothermodynamic Testing of the Crew Exploration Vehicle at Mach 6 and Mach 10. J Spacecraft Rockets 2009;46(4):758–65. https://doi.org/10.2514/ 1.39247
- [9] Thakre, P., Yang, V.: Chemical erosion of carbon-carbon/graphite nozzles in solidpropellant rocket.
- [10] Di Martino, G.D., Mungiguerra, S., Cecere, A., Savino, R., Zoli, L., Vinci, A., Silvestroni, L., Sciti, D.: Ultra-High-Temperature Ceramic Matrix Composites for

- Hybrid Rocket Nozzles, 70th International Astronautical Congress (IAC), IAC-19-C4.5.7.x50235, (2019).
- [11] Hald, H., Wehis, H., Safety Aspects of CMC Materials and Hot Structures, Proceedings of Joint ESA-NASA Space-Flight Safety Conference, ESTEC, Noordwijk (NI). (2002).
- [12] Liu L, Guo Q, He T. Thermal-Acoustic Fatigue of a Multilayer Thermal Protection System in Combined Extreme Environments. Adv Mech Eng 2014;6:176891.
- [13] Vassilopoulos AP. In: Fatigue Life Prediction of Composites and Composite Structures. Elsevier; 2010. p. 1–44.
- [14] Guiu F, Reece MJ, Vaughan DAJ. Cyclic fatigue of ceramics. J Mater Sci 1991;26: 3275–86. https://doi.org/10.1007/BF01124674.
- [15] Ruggles-Wrenn MB, Jones TP. Tension-compression fatigue of a SiC/SiC ceramic matrix composite at 1200°C in air and in steam. Int J Fatigue 2013;47:154–60. https://doi.org/10.1016/ji.jifatigue.2012.08.006.
- [16] Hou G, Shang D-G, Zuo L-X, Qu L-F, Xia M, Wu S, et al. Fatigue life prediction of needled ceramic matrix composite under variable amplitude loading. Int J Fatigue 2022;156:106690. https://doi.org/10.1016/j.ijfatigue.2021.106690.
- [17] Wolfe HF, Camden MP, Byrd LW, Paul DB, Simmons LW, Kim RY. Failure Criteria Development for Dynamic High-Cycle Fatigue of Ceramic Matrix Composites. J Aircraft 2000;37(2):319–24. https://doi.org/10.2514/2.2596.
- [18] Lugovy M, Orlovskaya N, Neubert M, Aneziris CG, Graule T, Kuebler J. Room temperature fatigue of ZrB2–SiC ceramic composites. Ceram Int 2013;39:9187–94. https://doi.org/10.1016/j.ceramint.2013.05.020.
- [19] Lugovy M, Orlovskaya N, Slyunyayev V, Mitrentsis E, Neumann M, Aneziris CG, et al. Comparative study of static and cyclic fatigue of ZrB2-SiC ceramic composites. J Europ Ceram Soc 2018;38(4):1128–35. https://doi.org/10.1016/j.jeurceramsoc.2017.12.024.
- [20] Zoli L, Sciti D, Vinci A, Galizia P, Monteverde F, Failla S, et al. Ultra-high temperature ceramic matrix composites. Encycl Mater Tech Ceram Glas 2021;2: 340–52. https://doi.org/10.1016/B978-0-12-818542-1.00023-0.

- [21] Galizia P, Vinci A, Zoli L, Monteverde F, Binner J, Venkatachalam V, et al. Retained strength of UHTCMCs after oxidation at 2278 K. Compos Part A Appl Sci Manuf 2021;149:106523. https://doi.org/10.1016/j.compositesa.2021.106523.
- [22] Sciti D, Galizia P, Reimer T, Schoberth A, Gutiérrez-Gonzalez CF, Silvestroni L, et al. Properties of large scale ultra-high temperature ceramic matrix composites made by filament winding and spark plasma sintering. Compos Part B Eng 2021; 216:108839. https://doi.org/10.1016/j.compositesb.2021.108839.
- [23] Mungiguerra S, Di Martino GD, Cecere A, Savino R, Silvestroni L, Vinci A, et al. Arc-jet wind tunnel characterization of ultra-high-temperature ceramic matrix composites. Corrosion Sci 2019;149:18–28. https://doi.org/10.1016/j. corsci.2018.12.039.
- [24] Baker B, Venkatachalam V, Zoli L, Vinci A, Failla S, Sciti D, et al. Ablation behaviour of carbon fibre ultra-high temperature composites at oblique angles of attack. Mater Des 2021;212:110199. https://doi.org/10.1016/j. matdes.2021.110199.
- [25] Servadei F, Zoli L, Vinci A, Galizia P, Sciti D. Significant improvement of the self-protection, capability of ultra-high temperature ceramic matrix composites. Corros Sci 2021;186:109575. https://doi.org/10.1016/j.corsci.2021.109575.
- [26] Vinci A, Reimer T, Zoli L, Sciti D. Influence of pressure on the oxidation resistance of carbon fiber reinforced ZrB2/SiC composites at 2000 and 2200 °C. Corros Sci 2021;184:109377. https://doi.org/10.1016/j.corsci.2021.109377.
- [27] Sciti D, Zoli L, Reimer T, Vinci A, Galizia P. A systematic approach for horizontal and vertical scale up of sintered Ultra-High Temperature Ceramic Matrix Composites for aerospace – Advances and perspectives. Compos Part B Eng 2022; 234:109709. https://doi.org/10.1016/j.compositesb.2022.109709.
- [28] Appert A, Gautrelet C, Khalij L, Troian R, Hénaff G. Development of a test bench for vibratory fatigue experiments of a cantilever beam with an electrodynamic shaker. MATEC Web of Conferences 2018;165:10007.
- [29] Ansys® Mechanical APDL, Release 2022 R2, Help System, Theory Reference, Chapter 15.7, ANSYS, Inc.